ORIGINAL PAPER

Non-Faradaic-based supercapacitor fabricated with fish skin gelatin biopolymer electrolyte

M. F. Z. Kadir [1]

Abstract

Fish gelatin (FS)–based polymer electrolytes doped with lithium perchlorate (LiClO$_4$) are prepared via the solution cast method. The ionic conductivity of undoped pure FS film has been identified to be $(9.29 \pm 0.89) \times 10^{-11}$ S cm^{-1} and increased to $(3.58 \pm 0.58) \times 10^{-6}$ S cm^{-1} with the inclusion of 25 wt.% LiClO$_4$ where this conductivity is mainly by ions due to the condition of $t_e < t_i$. X-ray diffraction (XRD) analysis showed that 25 wt.% LiClO$_4$ provides the most amorphous electrolyte. From the Fourier transform infrared (FTIR) spectroscopy, the shifting of amide A functional group peak indicates that cations from LiClO$_4$ have formed interaction with the polymer. FS-LiClO$_4$ electrolyte has been found to be electrochemically stable up to 1.88 V via linear sweep voltammetry (LSV). An electrical double-layer capacitor (EDLC) has been tested for 150 cycles where the specific capacitance at the 1st cycle is 28.2 F g^{-1}.

Keywords Fish skin gelatin · Lithium · Natural polymer · Energy storage · EDLC

Introduction

Solid polymer electrolytes are made in a polar polymer host by dissolving inorganic salt where metal ions from the salt form a coordinating bond with the polymer functional group of oxygen [1, 2]. Adding low molecular weight compounds to the polymer matrix can result in plasticized polymer electrolyte [3]. They have been proven to show a good performance in various modern electrochemical devices based on their morphological, electrical, and thermal properties [4]. Properties such as compatibility, flexibility, and capability of forming thin film media have made solid polymer electrolyte as an excellent alternative to liquid electrolyte due to no problem of leakage, thermally stable, and easy to be produced [5]. Moreover, natural polymers have a few important characteristics such as non-toxic and environmentally and economically friendly as well as abundant in nature [6, 7]. The biodegradable feature of these polymers makes it an ideal alternative to synthetic polymers that are not biodegradable. Natural polymers are commonly used in many sectors,

including medical [8], textile [9], cosmetic [10], and food packaging [11] industries.

Gelatin is one of the natural polymers and traditionally obtained by using the hydrolysis process of skin and bones from cattle and pigs which will lead to discomfort for the halal dietary restrictions community as well as pesco-vegetarians [12]. To solve this problem, gelatin also can be produced from fish because the fish industries have reported to produce a great amount of waste materials such as fish heads and skin [13]. Chitosan and fish gelatin can be obtained from these wastes which can minimize the environmental impacts [14, 15]. There is a huge amount of collagen that can be found in the fish skins and it is being commercialized as a food-grade gelatin. However, collagen content in cold water fish skin has fewer amounts of hydroxyproline and proline residues [16]. Besides, gelatin from marine sources showed lower functional properties, such as gelling temperature and gel strength than that of mammalian [17, 18]. The number of studies reported on the fish skin gelatin–based polymer electrolyte is still low.

Cations and anions are the ones responsible for the process of adsorption and desorption at the surface of the electrodes in an EDLC. Thus, salt doping has been employed by many researchers to improve the conductivity of the electrode separator. Lithium perchlorate (LiClO$_4$) has been chosen as the ion provider in this work for some reasons. As mentioned by Teoh et al. [19], LiClO$_4$ has a high diffusion rate and is comprised of

✉ M. F. Z. Kadir
mfzkadir@um.edu.my

[1] Centre for Foundation Studies in Science, University of Malaya, 50603 Kuala Lumpur, Malaysia

large anion and small cation. LiClO$_4$ has good conductivity and ease of complex formation in the fabrication of solid polymer electrolytes. LiClO$_4$ has lower lattice energy which 715 kJ mol^{-1} compared to other lithium salts e.g. lithium tetrafluoroborate (LiBF$_4$) (749 kJ mol^{-1}) and lithium acetate (LiOAc) (786 kJ mol^{-1}) [20]. More free ions can be produced with low lattice energy salts. Basu et al. [21] reported that LiClO$_4$ is compatible with gelatin-based polymers and the dielectric properties of the polymer electrolytes are enhanced with the presence of LiClO$_4$.

The increase of demand for renewable and high-performance energy devices is one of the current requirements of the human lifestyle that are focusing on a clean environment. Electrochemical double-layer capacitor (EDLC) can be used to replace conventional batteries which are now serving as the main choice to the community [22]. The EDLC uses a non-Faradaic process as an energy storage mechanism where only charge accumulation occurred and double-layer will form between the electrode surfaces as well as the interfacial region [23, 24]. To fabricate an EDLC, few methods have been widely studied to produce the electrode such as using carbon aerogel [25], graphite [26], and activated carbon [27]. However, activated carbon shows better characteristics and also has been extensively used in the electrochemical device field. This is because activated carbon has a reasonable price, better chemical stability, and large surface area as well as high electronic conductivity [28]. Moreover, EDLC has been a main option among the other supercapacitors due to simple fabrication method and has high durability, thermal stability, and power densities [29–31].

Experimental

Preparation of electrolyte

An amount of 2 g gelatin from cold-water fish skin (FS) (SIGMA) was stirred in 100 mL of distilled water at 60 °C for 30 min. The FS solution was cooled to room temperature before various amounts of LiClO$_4$ (SYSTERM) were added to produce salted electrolytes. Upon dissolution, FS-LiClO$_4$ solution was poured into a plastic Petri dish and left to dry in a fume hood at room temperature (25 °C, RH ~ 50%). The formed film was placed in a dessicator filled with silica gel to remove excess moisture before any characterization. The thickness of the film ranged from 0.022 to 0.035 cm. The designation of each electrolyte depends on the weight percentage (wt.%) of LiClO$_4$; e.g., the designation for electrolyte with 0, 5, 10, 15, 20, and 25 wt.% LiClO$_4$ was FS0, FS5, FS10, FS15, FS20, and FS25, respectively. Figure 1 shows the image of the highest conducting electrolyte film.
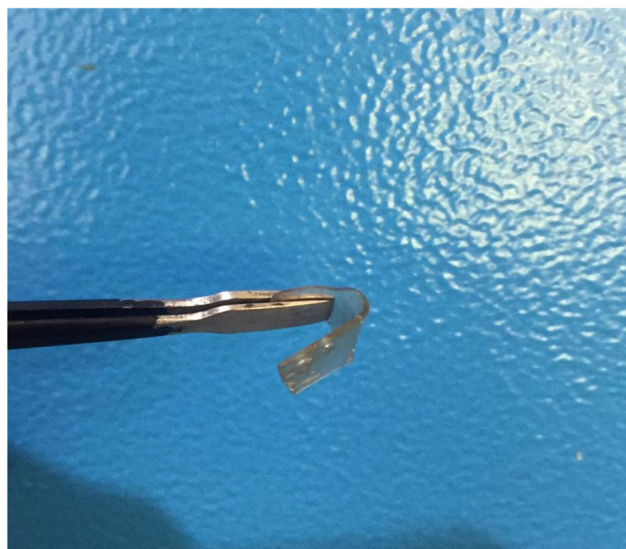

Fig. 1 The flexible highest conducting sample

Characterization of electrolyte

The conductivity and dielectric properties of the electrolyte were obtained using electrical impedance spectroscopy (EIS) measurements. EIS was performed using HIOKI 3532–50 LCR HiTESTER with a frequency range between 50 Hz and 5 MHz at room temperature. The cell arrangement was stainless steel (SS)| electrolyte | SS. The bulk resistance (R) of the electrolyte was extracted from the Nyquist plots. The conductivity value was identified using the following equation:

$$\sigma = \frac{t}{RA} \tag{1}$$

where A is the electrode-stainless steel contact area and t is the thickness of the electrolyte which was measured using Mitutoyo micrometer screw gauge. The real (ε_{re}) and imaginary (ε_{im}) parts of the dielectric permittivity (ε^*), which were recognized as dielectric constant and dielectric loss respectively, are extracted from:

$$\varepsilon_{re} = \frac{Z_{im}}{\omega C_o \left((Z_{re})^2 + (Z_{im})^2 \right)} \tag{2}$$

$$\varepsilon_{im} = \frac{Z_{re}}{\omega C_o \left((Z_{re})^2 + (Z_{im})^2 \right)} \tag{3}$$

where Z_{re} is the real part of impedance, Z_{im} is the imaginary part of impedance, ω stands for the radial frequency, and vacuum capacitance is given as C_o.

Fourier transform infrared (FTIR) spectroscopy was performed using a spectrometer (Spotlight 400 Perkin-Elmer) from 450 to 4000 cm^{-1} (resolution = 1 cm^{-1}). The image of electrolyte surface was captured using the Hitachi SU8220

FESEM with ×10k magnification. Thermogravimetric analysis (TGA) was performed using STA 6000 Perkin Elmer from room temperature to 970 °C at a heating rate of 20 °C min^{-1}. X-ray diffraction (XRD) analysis was conducted using a Siemens D5000 X-ray diffractometer (1.5406 Å) with a resolution of 0.1° ($2\theta = 5°$ to 80°). Deconvolution analysis was conducted using the Origin 9.0 software to separate amorphous and crystalline peaks from the raw XRD data where the degree of crystallinity (χ_c) and crystallite size (D_c) can be obtained using the following equations:

$$\chi_c = \frac{A_c}{A_c + A_a} \times 100\% \tag{4}$$

$$D_c = \frac{0.94\lambda}{FWHM\cos\theta} \tag{5}$$

where the areas of crystalline and amorphous peaks are given as A_c and A_a, respectively. λ is the X-ray wavelength (1.54 Å), and FWHM is the full-width half-maximum of the selected crystalline peak which was determined together during the deconvolution analysis.

V&A Instrument DP3003 digital DC power supply was used to perform the transference number (TNM) analysis via DC polarization method. The cell was polarized at 0.2 V. The DC current was monitored as a function of time at room temperature. The potential stability of the electrolyte was determined using linear sweep voltammetry (LSV) analysis. DY2300 potentiostat was used at 10 mV s^{-1} from 0 to 2.5 V. The cell arrangement for both TNM and LSV was the same as EIS analysis. The value of ionic (t_i) and electronic (t_e) transference number can be obtained from the following equations:

$$t_i = \frac{I_b - I_s}{I_b} \tag{6}$$

$$t_e = 1 - t_i \tag{7}$$

Fabrication and characterization of the fabricated EDLC

Step 1 was the dry mix process where 6.5 g activated carbon (AC) (Kuraray) and 0.5 g carbon black (CB) (Magna value) was mixed using planetary ball miller at 5 revolutions min^{-1} for 20 min. Step 2 was to dissolve 1 g of polyvinylidene fluoride (PVdF) (Magna value) in 30 mL of N-methyl-2-pyrrolidone (NMP) (EMPLURA). Step 3 was to dissolve the AC-CB powder in PVdF-NMP solution for several hours until homogenous black slurry was obtained. Step 4 was to clean the aluminum foil with acetone (SYSTERM) and coat the slurry using a doctor blade. The thickness of the electrode was set as 25 mm. Step 5 was to dry the coated aluminum foil in the oven at ~ 60 °C for several hours. The last step of electrode preparation was to cut the dried

electrode into a small circle shape with an area of 2.01 cm^2 and place the electrodes in desiccators to remove excess moisture. The most conductive sample was sandwiched in between electrodes and packed in CR2032 coin cells. The illustration of the fabricated EDLC was shown in Fig. 2. Cyclic voltammetry (CV) was performed with potential ranged from 0 to 0.9 V ($V_2 - V_1$) using Digi-IVY DY2300. The capacitance (C) of the EDLC can be expressed as:

$$C = \int_{V_1}^{V_2} \frac{I(V)dV}{2mS_r(V_2 - V_1)} \tag{8}$$

here, $I(V)dV$ is the area of CV plot that is extracted from the Origin 9.0 software, S_r is the scan rate, and m is the mass of the activated carbon which is an active material.

Results and discussion

XRD study

XRD analysis enables us to study the structure of a material. Figure 3 illustrates the effect of LiClO$_4$ addition on the crystallinity of the fish skin film. Raut et al. [32] stated that amorphous regions are preferable for ionic conduction in semi-crystalline polymers. Only a broad peak centered at 19.9° can be observed in FS0 (pure fish skin gelatin film) XRD pattern. This XRD pattern is common for gelatin-based film and comparable with other gelatin-based film studies [33, 34]. Das et al. [35] reported that the gelatin XRD pattern usually has a small crystalline peak at 7.0–8.1° and broad amorphous peak 19°. The peak at 7.0–8.1° in gelatin typically assigned to the triple-helical crystalline
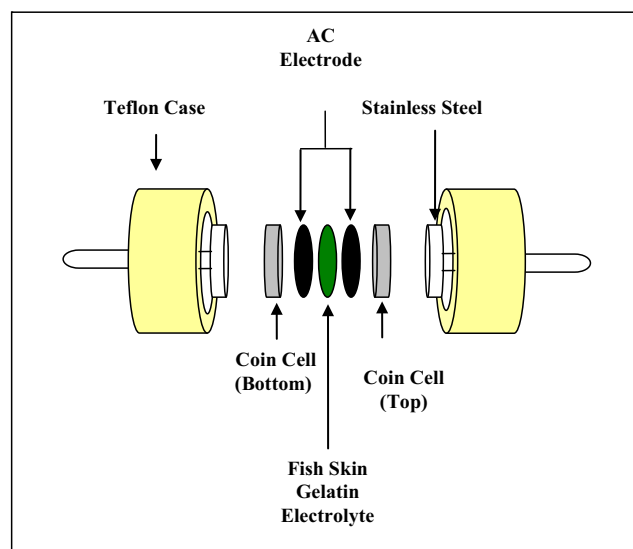

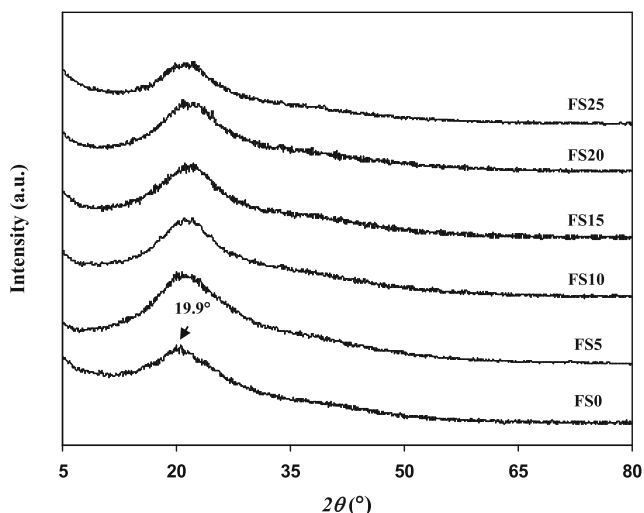**Fig. 2** The fabricated fish skin gelatin–based EDLC

Fig. 3 XRD patterns of FS-LiClO₄ system at various concentration of LiClO₄

structure [36]. The absence of this peak in FS0 XRD pattern could be due to the reduction of hydrogen bonding between polymer molecules with the presence of water and heat during sample preparation. This condition reduces the crystallinity of the FS film. The intensity of broad peak at 19.9° is reduced as 15 wt.% LiClO₄ is dope to FS film. As the concentration of LiClO₄ increases to 25 wt.%, the peak (19.9°) has become less sharp and broader compared to other compositions. It is reported that the addition of LiClO₄ into chitosan-dextran host has changed the XRD plot from a sharp shape to a broader shape [37]. This result indicates that more ions have built complexation with functional groups of FS film which will indirectly improve the ionic conductivity. The addition of lithium tetrafluoroborate ($LiBF_4$) into natural rubber polymer increased the amorphousness of the polymer electrolyte [38]. Furthermore, the absence of LiClO₄ sharp crystalline peaks indicates that the salt is completely dissolved in FS film.

Figure 4 portrays the deconvoluted XRD patterns of salted electrolytes. In XRD pattern of FS0, two peaks can be observed at $2\theta = 19.5°$ and $22.5°$. The addition of 10 wt.% LiClO₄ has reduced the intensity and increased the FWHM

of the crystalline peaks where the pattern continues as 25 wt.% LiClO₄ is added. The crystalline peaks of FS25 are broader compared to other concentrations. Based on this information, values of χ_c and D_c are obtained and tabulated in Table 1. Both χ_c and D_c of FS0 have reduced from 22.22% and 2.93 nm to 6.38% and 2.45 nm, respectively, as 25 wt.% LiClO₄ is added. This is due to the disruption of the crystalline structure of dextran by the presence of salt. Free ions from the salt form interactions with the functional groups of the polymer host via a dative bond, thus increasing the amorphousness of the electrolyte [39].

FTIR study

FTIR analysis is used by many researchers to observe interactions within the electrolyte where the shifting of peaks or

Table 1 Parameters obtained from the deconvolution analysis of XRD patterns.

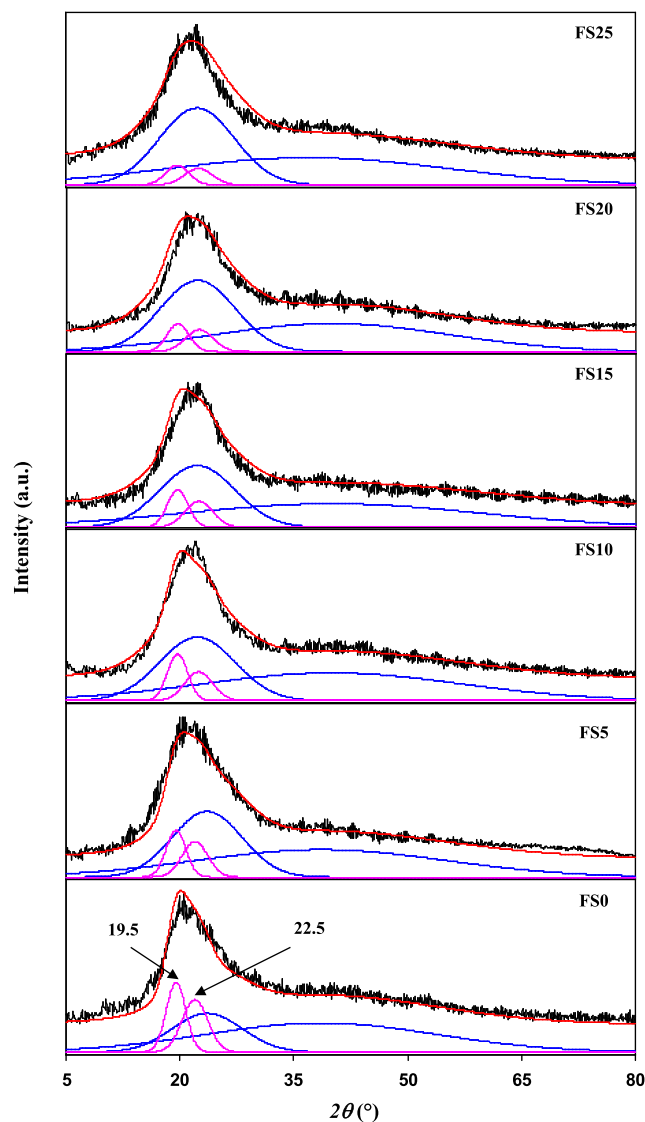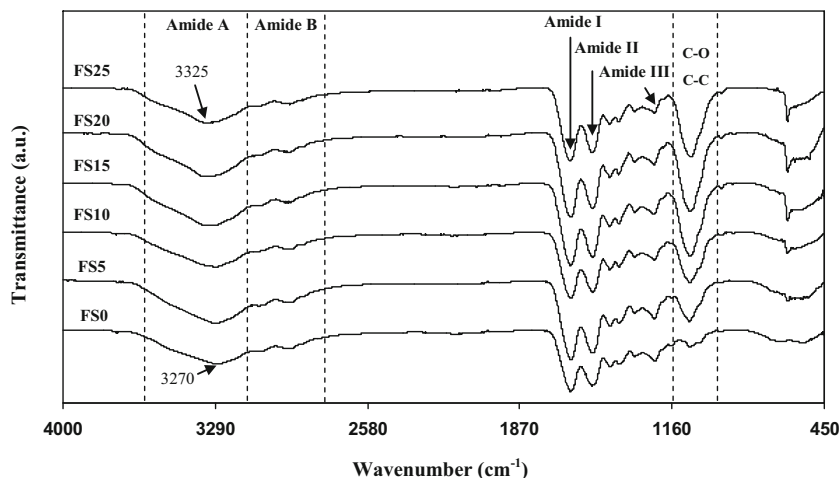| Electrolyte	FWHM for 19.5°	χ_c (%)	D_c (nm)
FS0	3	22.22	2.93
FS5	3.05	14.04	2.89
FS10	3.1	12.62	2.84
FS15	3.2	11.42	2.75
FS20	3.4	9.26	2.59
FS25	3.6	6.38	2.45

Fig. 4 Deconvoluted XRD plot of FS-LiClO₄ system with experimental (black), fitted (red), amorphous peak (blue), and crystalline peak (pink)

Fig. 5 FTIR spectra of the FS film with various amount of LiClO$_4$

changes in the intensity of a peak is considered as interactions. Figure 5 shows the FTIR spectra for the FS-LiClO$_4$ system from 450 to 4000 cm^{-1}. It is well known that any structure that is associated with protein will show several types of amide bands. The existence of these bands is from the vibrational motions of peptide bonds which connect together the amino acids that constitute the protein, in this case, the gelatin. The amide bands consisted of amide A (3500–3100 cm^{-1}), amide B (2800–3000 cm^{-1}), amide I (1630 cm^{-1}), amide II (1522 cm^{-1}), and amide III (1236 cm^{-1}) [40]. Amide A indicates the interaction between N–H stretching with hydrogen bonding and free OH [41]. As observed, the peak of amide A of FS0 has shifted from 3270 to 3325 cm^{-1} as 25 wt.% LiClO$_4$ is added. This situation means that cations (Li$^+$) from the salt have formed complexation with oxygen and nitrogen atoms in amide A. Amide B is C–H antisymmetric and symmetric stretching in aliphatic compounds [42]. Amide I is associated with the stretching vibrations of the C=O bond of the amide bond [43] while amide II is related to the bending vibrations of the N–H bond [44]. Amide III is due to C–N stretching vibrations coupled to N–H in-bending vibrations of the bound amide with weak contributions from C–C stretching [45]. It is noticeable that the peak of vibrational motions of C–O and C–C moieties (1072 cm^{-1}) increases with the addition of more LiClO$_4$. Thus, salt-polymer interactions in FS-LiClO$_4$ mostly happen in amide A and C–O regions.

Conductivity study

The segmental motion of the polymer chain depends on the free volume availability, glass transition temperature of the system, amount of salt, plasticizer, and fillers. These parameters affect the free volume of the polymer [46]. Thus, the effect of LiClO$_4$ addition on ionic conductivity of FS film is portrayed in Fig. 6. A low conductivity of $(9.29 \pm 0.89) \times 10^{-11}$ S cm^{-1} can be observed for pure FS film. This is due to the lack of ionic number density and polymers which are

known to possess insulator behavior. The addition of 15 wt.% LiClO$_4$ into the polymeric network has improved the conductivity up to 3 magnitude orders. This verifies that ions from LiClO$_4$ have interacted with complexation site of FS film [47]. The conductivity value of FS film is further increased to $(3.58 \pm 0.58) \times 10^{-6}$ S cm^{-1} with the presence of 25 wt.% LiClO$_4$. More charge carriers are provided at a high salt concentration which indirectly improves the ionic conductivity. The pattern of conductivity is consistent with the result from the FTIR study. Sangeetha et al. [48] reported a conductivity of 1.2×10^{-9} S cm^{-1} as 20 wt.% LiBF$_4$ is added to PVdF-HFP host. The presence of 30 wt.% LiOAc in PEO matrix provides a conductivity of 2.18×10^{-6} S cm^{-1} [49]. These reported conductivity values are lower than this work where one of the reasons is due to the difference in lattice energy values. Ion dissociation is easier for salt with low lattice energy where more free ions can be produced that will enhance the ionic conductivity. The conductivity trend is consistent with XRD analysis where as more LiClO$_4$ is added, the polymer
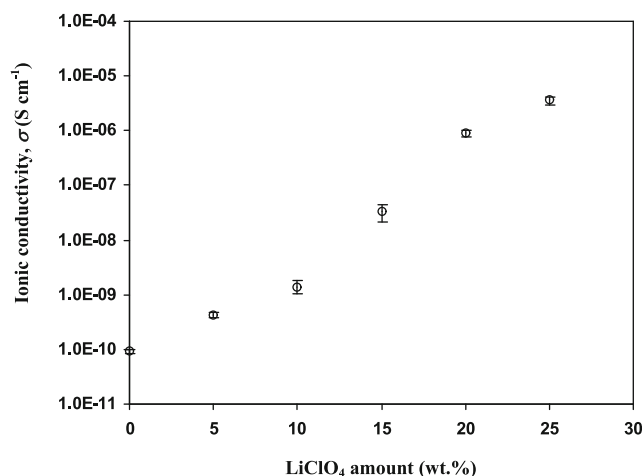

Fig. 6 Various ionic conductivity values at different concentration of LiClO$_4$

electrolyte becomes more amorphous and FS25 possesses the lowest crystallinity.

FESEM study

FESEM micrographs of the selected electrolytes are shown in Fig. 7. It can be seen that the surface of FS0 (pure fish gelatin) film is smooth and homogeneous, without pores or cracks. This result is similar to pure fish gelatin film surface reported by Qiang et al. [50]. As 10 wt.% $LiClO_4$, the surface turns to a rough structure with the presence of particles. Bhad and Sangawar [51] stated that these particles act as the channels for ionic conduction and considered evidence of salt-polymer interactions. However, as 25 wt.% $LiClO_4$ is included, the surface has changed to a denser structure indicating that the electrolyte has become more amorphous. This outcome infers that the polymer segmental has been improved with the presence of salt where it aids in the conduction of ions. This result is harmonized with conductivity and XRD result for FS25 where it has the highest conductivity value and the XRD shape is the broadest.

TGA study

The effect of salt doping on the thermal stability of a polymer film can be obtained using TGA analysis. Figure 8 shows the TGA thermograms for FS0 and FS25 from 25 to 970 °C. Two curves can be seen in each thermogram, one is the percentage of weight loss and the other one is the first derivative. The peak of the first derivative indicates the point of the greatest
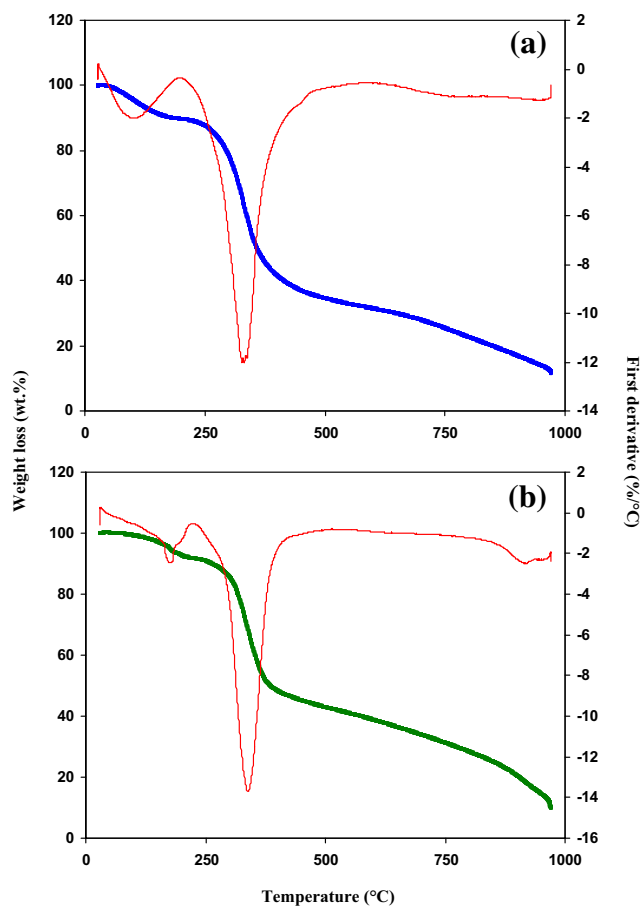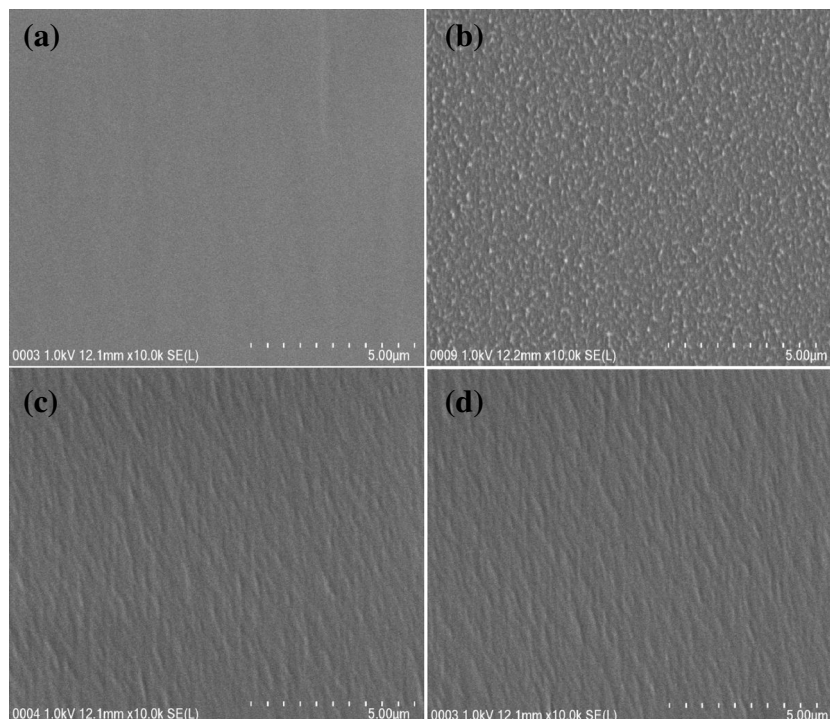

Fig. 8 TGA thermograms of **a** FS0 and **b** FS25

Fig. 7 Surface morphology of **a** FS0, **b** FS10, **c** FS20, and **d** FS25

rate of change on the weight loss curve or sometimes called as an inflection point. The 1st weight loss below 100 °C in FS0 thermograms is due to the weight loss of water as polymer possesses hydroscopic nature [52]. The 2nd weight loss of FS0 (54 %) has a larger first derivative peak compared to the first weight loss. This means that most weight loss happens in this region which is from 210 to 464 °C in FS0. Shehab et al. [53] reported that decomposition in this region is attributed to the loss of gelatin molecules. As 25 wt.% LiClO$_4$ is added as shown in Fig. 7b, the decomposition temperature has reduced to 150 °C where the weight loss is 7%. This is due to the disruption of hydrogen bond between polymer chains by the presence of salt [54]. As reported in Manap et al. [55], the decomposition temperature of poly(lactic acid)-poly(propylene glycol) has decreased with the addition of 15 to 30 wt.% LiClO$_4$. The 2nd weight loss in the thermogram of FS25 is due to the degradation of the gelatin.

Dielectric study

The dielectric study is a powerful tool to check the mechanism of ion transportation and the phase transitions within polymer electrolytes. Figure 9 a and b show the dielectric constant and dielectric loss, respectively, at various LiClO$_4$ concentrations. The dielectric constant is observed to increase as more salt is added. There are several bonds in a polymer, e.g., hydrogen
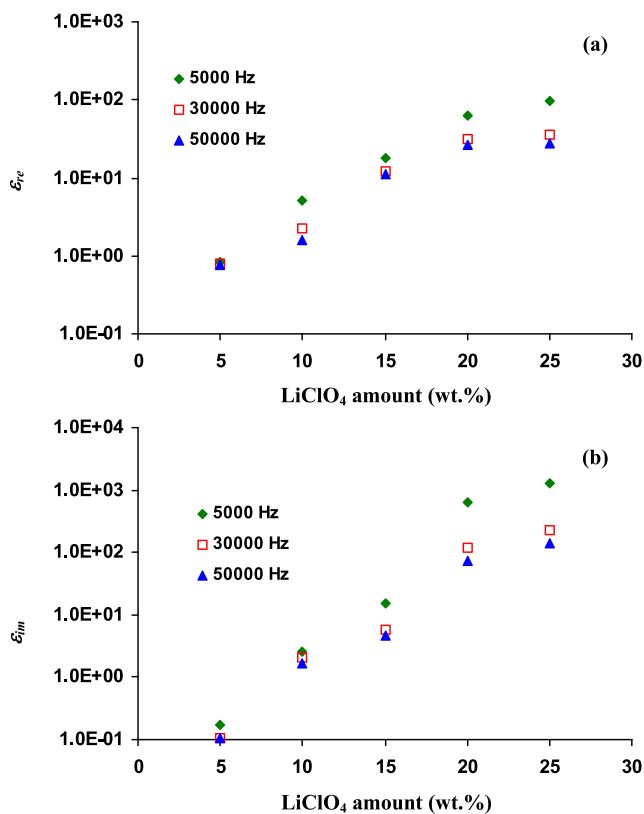
bonding (0.13–0.30 eV), dipolar interactions (0.07–0.13 eV), and dispersion interactions (0.002–0.09 eV) that can be disrupted with the presence of salt. The addition of salt affects the segmental motion of the polymer chain which can lead to more development of double-layer capacitance [56]. Dielectric loss in Fig. 9b also has the same increasing pattern. As more salt is added, more free ions undergo conduction towards the electrodes. During this transport time, ion collides with other ion and this collision cause some energy loss. Thus, when there are more ions, more energy loss will be produced [57]. Other than that, dielectric is higher at 50 Hz compared to 30,000 and 50,000 Hz. At low frequency, it is easier for ions to obey the changes of the electric field and form a proper charge double-layer. Meanwhile, incomplete polarization at high frequency occurs due to the rapid and unstable movement of ions [58]. The conductivity trend is consistent with the pattern of dielectric constant and loss.

TNM study

To use the polymer electrolyte in energy storage devices, it is crucial to examine the transference number of both ions and electrons. Some electrical devices are dependent on electrons flow, e.g., semiconductor and solar cell. Typically, in a conventional battery, cations are responsible for the process of intercalation and deintercalation. However, in EDLC, ions are the ones in charge of storing energy. Thus, high ionic contribution is a must in EDLC application (>0.90). It is noticeable in Fig. 10 that the current is large at the beginning which is at this point both ions and electrons are conducted. As time goes by, ions are blocked at the surface of the electrodes and at this point the cell is polarized where the current flows are due to the electrons [59]. t_i for the best conducting sample of FS-LiClO$_4$ system is found to be 0.97. This value is sufficient enough and near the unity value to make the electrolyte become useful in EDLC application. Gohel et al. [60]
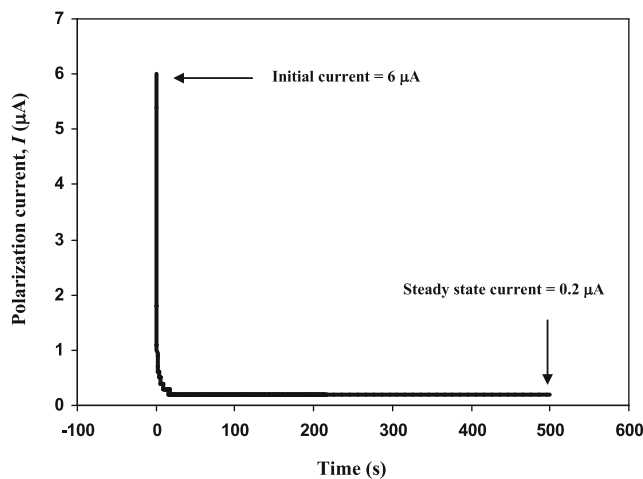
Fig. 9 Plot of the **a** real and **b** imaginary part of the dielectric

Fig. 10 Polarization current versus time for F25 at 0.2 V

reported that t_i in the PVdF-PMMA-LiClO$_4$ system ranged from 0.96 to 0.99. A series of t_i from 0.85 to 0.89 for PEO-LiClO$_4$-ZnO system is reported by Patil et al. [61].

LSV study

The potential stability (i.e., working cell potential range) of polymer electrolytes is a vital parameter to be determined for their implementation in energy storage devices. The potential stability window of F25 is evaluated using linear sweep voltammetry (LSV) analysis, and its corresponding voltammogram is depicted in Fig. 11. It can be seen that there is no current flows through the working electrode below ~ 1.50 V. The cell is polarized at this stage. At potential below ~ 1.50 V, the increment of current value is slow. However, as the potential increased to more than 1.88 V, the current increase drastically. A sharp increase in the current marks the starting of electrolyte decomposition. This outcome confirms that FS25 with the best conductivity in this work is potentially stable up to 1.88 V; thus, it is suitable for EDLC application. A work of chitosan-LiCO$_2$CH$_3$-glycerol system has been reported to possess potential stability of 1.80 V [62]. Chandra et al. [63] reported the potential stability of PVA-PMMA-LiCl is up to 1.69 V.

CV study of the fabricated EDLC

The energy storage mechanism of an EDLC is through adsorption/desorption process instead of intercalation/deintercalation where this mechanism can be verified via CV analysis. Figure 12a illustrates the CV plot of the constructed EDLC at different scan rates. No peaks can be observed in CV plots of all scan rates. This verifies that the EDLC in this work obeys the typical energy storing mechanism of a capacitor which is non-Faradaic process [64]. The CV plot at 100 mV s^{-1} is a leaf-like shape where it changes to more rectangular shape as the scan rate reduces to 10 mV s^{-1}. It is common that
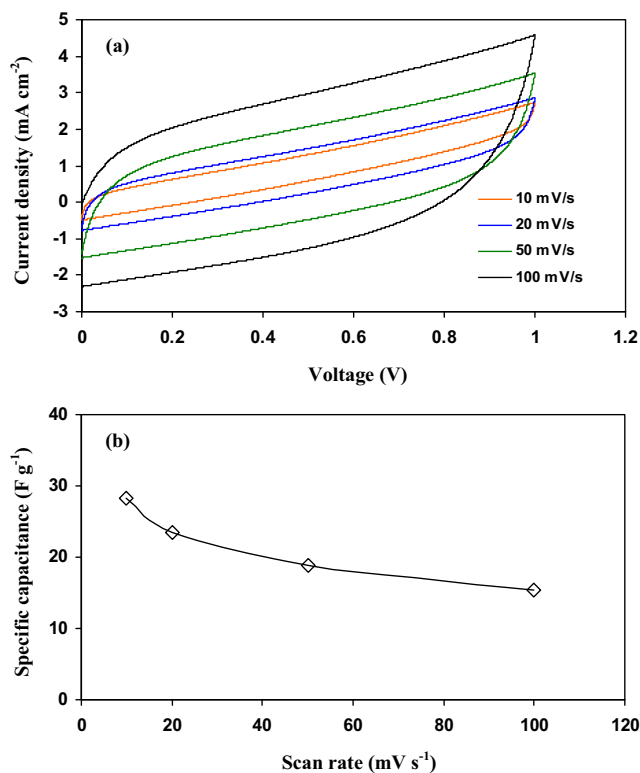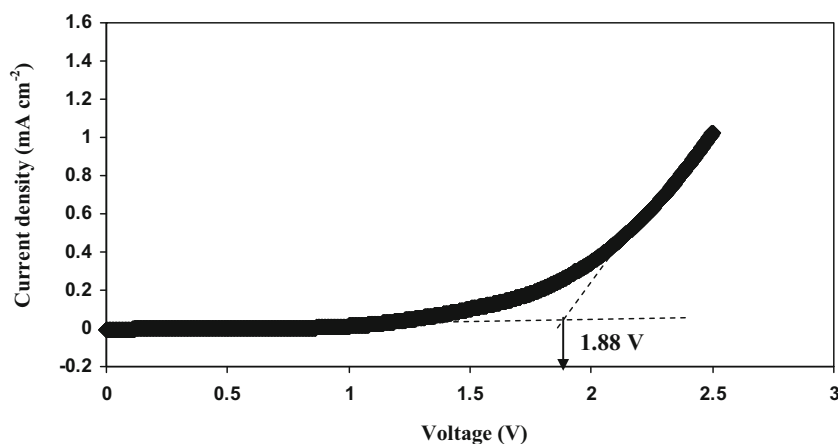

Fig. 12 **a** CV plot of the EDLC and **b** specific capacitance at different scan rates

CV for a capacitor is scan rate–dependent. The migration of charge carriers occurs at a rapid rate at a high scan rate. In addition, due to carbon porosity and internal resistance, current dependence of voltage is produced [65]. As observed in Fig. 12b, the value of C achieved is 15.3 F g^{-1} for 100 mV s^{-1}, meanwhile, 28.2 F g^{-1} for 10 mV s^{-1}. Ions are able to move at a stable rate when a low scan rate is employed; thus, they can form more and properly charged double-layer. At a high scan rate, ions are migrated at a very fast rate; this situation decreases the formation of charge double-layer which reduces the capacitance value [66, 67].

Fig. 11 LSV plot of FS25 at a scan rate of 10 mV s^{-1}

The cycleability of the EDLC is analyzed using a scan rate of 10 mV s^{-1} for 150 cycles. In Fig. 13a, the CV plot has a rectangular-like shape for the first 50 cycles where the shape has changed to a leaf-like shape from 75th to 150th cycles in Fig. 13b. As the cycle number increases, some of the free ions undergo a recombination process to form ion pairs. These ion pairs disturb the process of charge double-layer development and thus, the current is dependent on the voltage. Figure 13c shows the calculated value of C throughout the 150 cycles. The value of C at the 1st cycle is 28.1 F g^{-1} which is similar to the result in Fig. 13b where the value of C is 28.2 F g^{-1} at 10 mV s^{-1}. C then increases to 34.7 F g^{-1} at the 15th cycle. Stabilization is achieved at an average of 39.0 F g^{-1} from 25th to 60th cycle. At this stage, ions experience a constant rate of double-layer development where it is correlated to the rectangular shape of the CV plot for cycles < 50. As the cycle number exceeded 60, the value decreases to an average of 34.0 F g^{-1} from 70th to 100th cycle. Beyond 100th cycles, the value of C reduces to 19.7 F g^{-1} at 150th cycles. The decrement in the C value is due to the increment in the ion recombination process that obstructs the pathway of free ions to perform polarization at the surface of activated carbon. Table 2 shows various electrolyte systems-based EDLCs reported by other researchers.

Conclusion

Fish skin gelatin-LiClO$_4$–based natural polymer electrolytes have been successfully prepared using the solution casting method. XRD analysis verifies that the presence of LiClO$_4$ has improved the amorphousness of the electrolyte as the highest conducting sample possessed the lowest crystallinity and crystallite size. The proof of polymer-Li$^+$ interaction has been proven as the inclusion of LiClO$_4$ has further shifted the peak of amide A and C–O bands via FTIR analysis. The inclusion of 25 wt.% LiClO$_4$ has increased the conductivity

Table 2 Reported EDLCs with their respective polymer electrolyte and specific capacitance

Polymer electrolyte	Scan rate (mV s^{-1})	C (F g^{-1})	Reference
PVA-CH$_3$COONH$_4$	10	0.14	[66]
PVA-LiClO$_4$	10	3.2	[68]
Starch-LiClO$_4$	10	5.42	[69]
Corn Starch-LiClO$_4$-BaTiO$_3$	-	16.22	[70]
PEO/NPPP-LiClO$_4$	5	17.4	[71]
HEC-Mg(CF$_3$SO$_3$)$_2$	5	21.4	[72]
EC-DMC-LiTFSI	5	24.0	[73]
FS-LiClO$_4$	10	28.1	This work
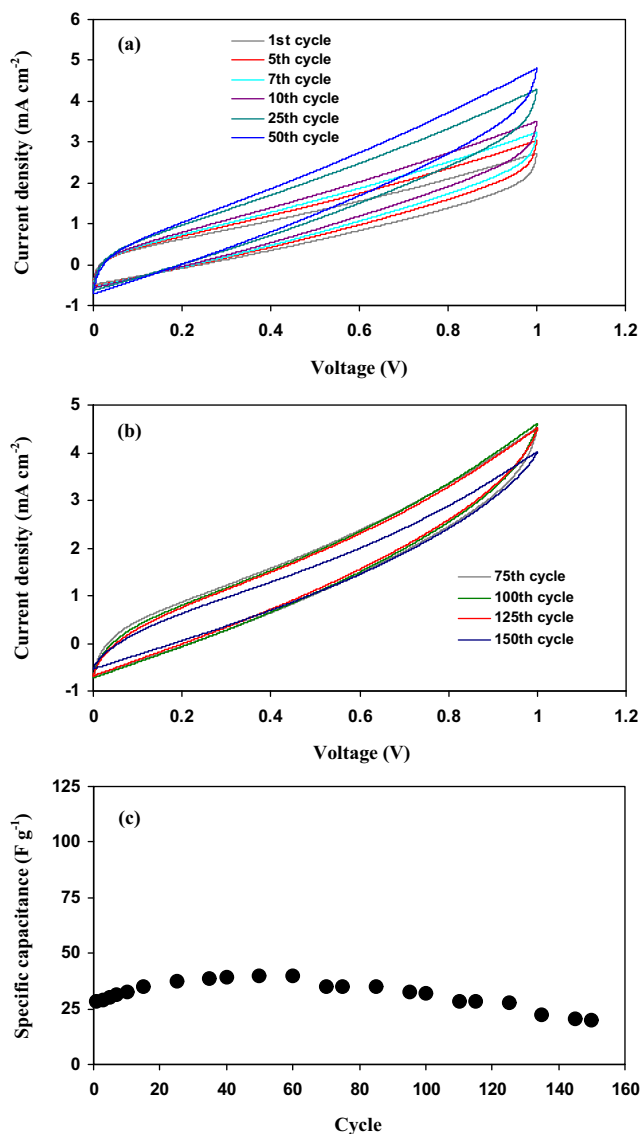
Fig. 13 CV plot of the EDLC at 10 mV s^{-1} for **a** 1st to 50th cycle and **b** 75th to 150th cycle. **c** Specific capacitance of the EDLC at selected cycles

value from 10^{-11} to 10^{-6} S cm^{-1}. From the dielectric study, it is identified that the existence of LiClO$_4$ has increased the dielectric constant of the electrolyte where it is harmonized with the pattern of ionic conductivity. The thermal stability of the polymer electrolytes is reduced by the addition of LiClO$_4$. Ions have been found to be the primary charge carriers as 0.97 was achieved for the ionic transference number (t_i). FESEM study showed that the surface of the electrolyte has turned to a denser structure. FS-LiClO$_4$ was found to be potentially safe below 1.88 V from LSV analysis. The shape of the CV plot was changed throughout the 150 cycles and the specific capacitance obtained at the 1st cycle was 28.2 F g^{-1}. Many aspects have to be considered to improve the performance of the EDLC, e.g., electrodes and electrolytes. For electrolytes, plasticizer and nanofiller can be added to reduce the resistance of the electrolyte. Hence, more ions are available to form a

charge double layer. Modification of electrodes such as using less binder that increases the resistance of the electrode can increase the conductivity of the electrodes. The employment of carbon electrodes like carbon nanotubes, carbon aerogel, and graphite might enhance the performance of the EDLC.

References

1. Rivas BL, Maureira A, Guzma'n C, Mondaca MA (2009) Poly(2-acrylamido glycolic acid-co-2-acrylamido-2- methyl-1-propane sulfonic acid): synthesis, characterization, and retention properties for environmentally impacting metal ions. J Appl Polym Sci 111:78–86

2. Aziz SB, Woo HJ, Kadir MFZ, Ahmed HM (2018) A conceptual review on polymer electrolytes and ion transport models. J Sci Adv Mater Devices 3:1–17

3. Stephan AM, Kumar TP, Kulandainathan MA, Lakshmi NA (2009) Chitin-incorporated poly(ethylene oxide)-based nanocomposite electrolytes for lithium batteries. J Phys Chem B 113:1963–1971

4. Aziz SB, Abidin ZHZ, Kadir MFZ (2015) Innovative method to avoid the reduction of silver ions to silver nanoparticles. Phys Scr 90:1–9

5. Lin YC, Ito K, Yokoyama H (2018) Solid polymer electrolyte based on crosslinked polyrotaxane. Polym 136:121–127

6. Mostafa NA, Farag AA, Abo-dief HM, Tayeb AM (2018) Production of biodegradable plastic from agricultural wastes. Arab J Chem 11:546–553

7. Muthukrishnan M, Shanthi C, Selvasekarapandian S, Manjuladevi R, Perumal P, Chrishtopher Selvin P (2018) Synthesis and characterization of pectin-based biopolymer electrolyte for electrochemical applications. Ionics (Kiel) 25:203–214

8. Bin Park S, Lih E, Park KS, Joung YK, Han DK (2017) Biopolymer-based functional composites for medical applications. Prog Polym Sci 68:77–105

9. Younes B (2017) Classification, characterization, and the production processes of biopolymers used in the textiles industry. J Text Inst 108:674–682

10. Rebelo R, Fernandes M, Fangueiro R (2017) Biopolymers in medical implants: a brief review. Procedia Eng 200:236–243

11. Othman SH (2014) Bio-nanocomposite materials for food packaging applications: types of biopolymer and nano-sized filler, agric. Agric Sci Procedia 2:296–303

12. Sow LC, Yang H (2015) Effects of salt and sugar addition on the physicochemical properties and nanostructure of fish gelatin. Food Hydrocoll 45:72–82

13. Silva NDE, Pino Hernández EJG, Da Silva Araújo C, Peixoto Joele MRS, Lourenço LFH (2018) Development and optimization of biodegradable fish gelatin composite film added with buriti oil. CYTA - J. Food 16:340–349

14. Ocak B (2012) Complex coacervation of collagen hydrolysate extracted from leather solid wastes and chitosan for controlled release of lavender oil. J Environ Manag 100:22–28

15. Karim AA, Bhat R (2009) Fish gelatin: properties, challenges, and prospects as an alternative to mammalian gelatins. Food Hydrocoll 23:563–576

16. GoÂmez-GuilleÂn MC, Turnay J, FernaÂndez-DÕÂaz MD, Ulmo N, Lizarbe MA, Montero P (2002) Structure and physical properties of gelatin extracted from different marine species: a comparative study. Food Hydrocoll 16:25–34

17. Rattaya S, Benjakul S, Prodpran T (2009) Properties of fish skin gelatin film incorporated with seaweed extract. J Food Eng 95:151–157

18. Bower CK, Avena-Bustillos RJ, Olsen CW, McHugh TH, Bechtel PJ (2006) Characterization of fish-skin gelatin gels and films containing the antimicrobial enzyme lysozyme. J Food Sci 71:M141–M145

19. Teoh KH, Ramesh S, Arof AK (2012) Investigation on the effect of nanosilica towards corn starch–lithium perchlorate-based polymer electrolytes. J Solid State Electrochem 16:3165–3170

20. Singh TH, Bhat SV (2003) Morphology and conductivity studies of a new solid polymer electrolyte: (PEG)xLiClO4. Bull Mater Sci 26:707–714

21. Basu T, Goswami MM, Middya TR, Tarafdar S (2012) Morphology and ion-conductivity of gelatin-LiClO$_4$ films: fractional diffusion analysis. J Phys Chem B 116:11362–11369

22. Asnawi ASFM, Aziz SB, Nofal M, Abdulwahid RT, Kadir MFZ, Hamsan MH, Brza MA, Yusof YM, Abdilwahid RT (2020) Glycerolized Li + ion conducting chitosan-based polymer electrolyte for energy storage edlc device applications with relatively high energy density. Polym (Basel) 12:1–19

23. Iro ZS, Subramani C, Dash SS (2016) A brief review on electrode materials for supercapacitor. Int J Electrochem Sci 11:10628–10643

24. Shukur MF, Ithnin R, Illias HA, Kadir MFZ (2013) Proton conducting polymer electrolyte based on plasticized chitosan-PEO blend and application in electrochemical devices. Opt Mater (Amst) 35:1834–1841

25. Ling L, Qing-Han M (2005) Electrochemical properties of mesoporous carbon aerogel electrodes for electric double layer capacitors. J Mater Sci 40:4105–4107

26. Subramanian V, Zhu H, Wei B (2008) Nanostructured manganese oxides and their composites with carbon nanotubes as electrode materials for energy storage devices. Pure Appl Chem 80:2327–2343

27. Kadir MFZ, Majid SR, Arof AK (2010) Plasticized chitosan-PVA blend polymer electrolyte based proton battery. Electrochim Acta 55:1475–1482

28. Wang H, Lin J, Shen ZX (2016) Polyaniline (PANi) based electrode materials for energy storage and conversion. J Sci Adv Mater Devices 1:225–255

29. Inagaki M, Konno H, Tanaike O (2010) Carbon materials for electrochemical capacitors. J Power Sources 195:7880–7903

30. Zhang D, Zhang X, Chen Y, Yu P, Wang C, Ma Y (2011) Enhanced capacitance and rate capability of graphene/polypyrrole composite as electrode material for supercapacitors. J Power Sources 196:5990–5996

31. Pell WG, Conway BE (2004) Peculiarities and requirements of asymmetric capacitor devices based on combination of capacitor and battery-type electrodes. J Power Sources 136:334–345

32. Raut P, Li S, Chen YM, Zhu Y, Jana SC (2019) Strong and flexible composite solid polymer electrolyte membranes for Li-ion batteries. ACS Omega 4:18203–18209

33. Kwak HW, Woo H, Kim IC, Lee KH (2017) Fish gelatin nanofibers prevent drug crystallization and enable ultrafast delivery. RSC Adv 7:40411

34. Arfat YA, Ahmed J, Hiremath N, Auras R, Joseph A (2017) Thermo-mechanical, rheological, structural and antimicrobial properties of bionanocomposite films based on fish skin gelatin and silver-copper nanoparticles. Food Hydrocoll 62:191–202

35. Das MP, Suguna PR, Prasad K, Vijaylakshmi JV, Renuka M (2020) Extraction and characterization of gelatin: a functional biopolymer. Int J Pharm Sci 9:239–242

36. Peña C, Caba KDL, Eceiza A, Ruseckaite R, Mondragon I (2010) Enhancing water repellence and mechanical properties of gelatin films by tannin addition. Bioresource Tech 101:6836–6842

37. Aziz SB, Hamsan MH, Kadir MFZ, Karim WO, Abdullah RJ (2019) Development of polymer blend electrolyte membranes based on chitosan: dextran with high ion transport properties for EDLC application. Int J Mol Sci 20:3369

38. Ahmad A, Rahman MYA, Low SP, Hamzah H (2011) Effect of LiBF$_4$ salt concentration on the properties of plasticized MG49-TiO$_2$ based nanocomposite polymer electrolyte. ISRN 2011:1–7

39. Hassan MF, Azimi NSN, Kamarudin KH, Sheng CK (2018) Solid polymer electrolytes based on starch-magnesium sulphate: study on morphology and electrical conductivity. ASM Sci J 11:17–28

40. Pępczyńska M, Díaz-Calderón P, Quero F, Matiacevich S, Char C, Enrione J (2019) Interaction and fragility study in salmon gelatin-oligosaccharide composite films at low moisture conditions. Food Hydrocoll 97:105207

41. Pradini D, Juwono H, Madurani KA, Kurniawan F (2018) A preliminary study of identification halal gelatin using quartz crystal microbalance (QCM) sensor. Malaysian Mal J Fund Appl Sci 14:325–330

42. Kuan YH, Nafchi AM, Huda N, Ariffin F, Karim AA (2016) Effects of sugars on the gelation kinetics and texture of duck feet gelatin. Food Hydrocoll 58:267–275

43. Ahmad M, Benjakul S (2011) Characteristics of gelatin from the skin of unicorn leatherjacket (Aluterus monoceros) as influenced by acid pretreatment and extraction time. Food Hydrocoll 25:381–388

44. Cebi N, Durak MZ, Toker OS, Sagdic O, Arici M (2016) An evaluation of Fourier transforms infrared spectroscopy method for the classification and discrimination of bovine, porcine and fish gelatins. Food Chem 190:1109–1115

45. Al-Saidi A, Rahman MS, Guizani N (2012) Fourier transform infrared (FTIR) spectroscopic study of extracted gelatin from shaari (Lithrinus microdon) skin: Effects of extraction conditions. Int Food Res J 19:1167–1173

46. Liao H, Hong H, Zhang H, Li Z (2016) Preparation of hydrophilic polyethylene/methylcellulose blend microporous membranes for separator of lithium-ion batteries. J Membrane Sci 498:147–157

47. Lim CS, Teoh KH, Ng HM, Liew CW, Ramesh S (2017) Ionic conductivity enhancement studies of composite polymer electrolyte based on poly (vinyl alcohol)-lithium perchlorate-titanium oxide. Adv Mat Lett 2017(8):465–471

48. Sangeetha M, Mallikarjun A, Jaipal RM, Kumar SJ (2017) SEM, XRD and electrical conductivity studies of PVDF-HFP-LiBF$_4$-EC plasticized gel polymer electrolyte. AIP Conf Proc 1859:020064

49. Ismail L, Majid SR, Arof AK (2009) Conductivity study in PEO–LiOAc based polymer electrolyte. Mat Res Innov 13:282–284

50. Qiang X, Zhou S, Zhang Z, Quan Q, Huang D (2018) Synergistic effect of halloysite nanotubes and glycerol on the physical properties of fish gelatin films. Polym 10:1258

51. Bhad SN, Sangawar VS (2013) Optical study of PVA based gel electrolyte. Int J Sci Eng Res 4:1719–1722

52. Les K, Jordan CS (2020) Ionic conductivity enhancement in solid polymer electrolytes by electrochemical in situ formation of an interpenetrating network. RSC Adv 10:41296–41304

53. Shehap AM, Mahmoud KH, Abd El-Kader MFH, EL-Basheer TM (2015) Preparation and thermal properties of gelatin/TGS composite films. Middle East J Appl Sci 5:157–170

54. Sanyang M, Sapuan SM, Jawaid M, Ishak MR, Sahari J (2015) Effect of plasticizer type and concentration on tensile, thermal and barrier properties of biodegradable films based on sugar palm (arenga pinnata) starch. Polym 7:1106–1124

55. Manap SM, Ahmad A, Sarjadi MS, Anuar FH (2019) Effect of plasticizers and lithium perchlorate on poly(llactic acid)-poly(propylene glycol) solid polymer electrolyte. Malaysian J Anal Sci 23:703–714

56. Das-Gupta DK (2001) Molecular processes in polymer electrolytes. J Electrost 515:159–166

57. Marf AS, Abdullah RM, Aziz SB (2020) Structural, morphological, electrical and electrochemical properties of PVA: CS-based proton-conducting polymer blend electrolytes. Membranes 10:71

58. Arya A, Sharma AL (2019) Tailoring of the structural, morphological, electrochemical, and dielectric properties of solid polymer electrolyte. Ionics 25:1617–1632

59. Tripathi M, Tripathi SK (2017) Electrical studies on ionic liquid-based gel polymer electrolyte for its application in EDLCs. Ionics 23:2735

60. Gohel K, Kanchan DK (2018) Ionic conductivity and relaxation studies in PVDF-HFP:PMMA-based gel polymer blend electrolyte with LiClO$_4$ salt. J Adv Dielectr 8:1850005

61. Patil SU, Yawale SS, Yawale SP (2014) Conductivity study of PEO–LiClO$_4$ polymer electrolyte doped with ZnO nanocomposite ceramic filler. Bull Mater Sci 371403-1409

62. Asnawi ASFM, Aziz SB, Nofal MM, Hamsan MH, Brza MA, Yusof YM, Abdilwahid RT, Muzakir SK, Kadir MFZ (2020) Glycerolized Li+ ion conducting chitosan-based polymer electrolyte for energy storage edlc device applications with relatively high energy density. Polym 12:1433

63. Chandra MVL, Karthikeyan S, Selvasekarapandian S, Premalatha M, Monisha S (2017) Study of PVAc-PMMA-LiCl polymer blend electrolyte and the effect of plasticizer ethylene carbonate and nanofiller titania on PVAc-PMMALiCl polymer blend electrolyte. J Polym Eng 37:617–631

64. Fattah N, Ng H, Mahipal Y, Numan A, Ramesh S, Ramesh K (2016) An approach to solid-state electrical double layer capacitors fabricated with graphene oxide-doped, ionic liquid-based solid copolymer electrolytes. Mater 9:450

65. Jäckel N, Rodner M, Schreiber A, Jeongwook J, Zeiger M, Aslan M, Weingarth D, Presser V (2016) Anomalous or regular capacitance? The influence of pore size dispersity on double-layer formation. J. Power Sources 326:660–671

66. Liew CW, Ramesh S, Arof AK (2016) Enhanced capacitance of EDLCs (electrical double layer capacitors) based on ionic liquid-added polymer electrolytes. Energy 109:546–556

67. Yadav N, Promila R, Hashmi SA (2020) Hierarchical porous carbon derived from eucalyptus-bark as a sustainable electrode for high-performance solid-state supercapacitors. Sustain Energy Fuels 4:1730–1746

68. Lim CS, Teoh KH, Liew C, Ramesh S (2014) Capacitive behavior studies on electrical double layer capacitor using poly (vinyl alcohol)-lithium perchlorate based polymer electrolyte incorporated with TiO$_2$. Mater Chem Phys 143:661–667

69. Teoh KH, Lim CS, Liew CW, Ramesh S, Ramesh S (2015) Electric double-layer capacitors with corn starch-based biopolymer electrolytes incorporating silica as filler. Ionics 21:2061–2068

70. Teoh KH, Lim CS, Liew CW, Ramesh S (2015) Preparation and performance analysis of barium titanate incorporated in corn starch-based polymer electrolytes for electric double layer capacitor application. J App Polym Sci 133:43275

71. Lavall RL, Borges RS, Calado HDR, Welter C, Trigueiro JPS, Rieumont J, Neves BRA, Silva GG (2008) Solid state double layer capacitor based on a polyether polymer electrolyte blend and nanostructured carbon black electrode composites. J Power Sources 177:652–659

72. Chong MYA, Numan A, Liew CW, Ramesh K, Ramesh S (2017) Comparison of the performance of copper oxide and yttrium oxide nanoparticle based hydroxylethyl cellulose electrolytes for supercapacitors. J Appl Polym Sci 134:44636

73. Nadiah N, Omar FS, Numan A, Mahipal Y, Ramesh S, Ramesh K Influence of acrylic acid on ethylene carbonate/dimethyl carbonate based liquid electrolyte and its supercapacitor application. Int J Hydrogen Energy 42:30683–30690